Paleobiology, 2021, pp. 1–16
DOI: 10.1017/pab.2021.7

PALEOBIOLOGY
A PUBLICATION OF THE Paleontological SOCIETY

Article

Photosymbiosis in planktonic foraminifera across the Paleocene–Eocene thermal maximum

Jack O. Shaw, Simon D'haenens, Ellen Thomas, Richard D. Norris, Johnnie A. Lyman, André Bornemann, and Pincelli M. Hull*

Abstract.—Under stress, corals and foraminifera may eject or consume their algal symbionts ("bleach"), which can increase mortality. How bleaching relates to species viability over warming events is of great interest given current global warming. We use size-specific isotope analyses and abundance counts to examine photosymbiosis and population dynamics of planktonic foraminifera across the Paleocene–Eocene thermal maximum (PETM, ~56 Ma), the most severe Cenozoic global warming event. We find variable responses of photosymbiotic associations across localities and species. In the NE Atlantic (DSDP Site 401) PETM, photosymbiotic clades (acarininids and morozovellids) exhibit collapsed size-$\delta^{13}C$ gradients indicative of reduced photosymbiosis, as also observed in Central Pacific (ODP Site 1209) and Southern Ocean (ODP Site 690) acarininids. In contrast, we find no significant loss of size-$\delta^{13}C$ gradients on the New Jersey shelf (Millville) or in Central Pacific morozovellids. Unlike modern bleaching-induced mass mortality, populations of photosymbiont-bearing planktonic foraminifera increased in relative abundance during the PETM. Multigenerational adaptive responses, including flexibility in photosymbiont associations and excursion taxon evolution, may have allowed some photosymbiotic foraminifera to thrive. We conclude that deconvolving the effects of biology on isotope composition on a site-by-site basis is vital for environmental reconstructions.

Jack O. Shaw, S. D'haenens†, Ellen Thomas‡, and Pincelli M. Hull. Department of Earth and Planetary Sciences, 21 Sachem Street, Yale University, New Haven, Connecticut 06511, U.S.A. E-mail: jack.shaw@yale.edu, pincelli.hull@yale.edu. Present address: †Research Coordination Office and Data Science Institute, Hasselt University, Agoralaan Building D, 3590 Diepenbeek, Belgium. E-mail: simon.dhaenens@scarlet.be. Also at: ‡Department of Earth and Environmental Sciences, Wesleyan University, Middletown, Connecticut 06459, U.S.A. E-mail: ellen.thomas@yale.edu

Richard D. Norris. Scripps Institution of Oceanography, University of California, San Diego, California 92093, U.S.A. E-mail: rnorris@ucsd.edu

Johnnie A. Lyman. High Tech High North County, 1420 West San Marcos Boulevard, San Marcos, California 92078, U.S.A. E-mail: johnnielyman@gmail.com.

André Bornemann.Bundesanstalt für Geowissenschaften und Rohstoffe, Stilleweg 2, 30655 Hannover, Germany. E-mail: andre.bornemann@bgr.de

*Corresponding author.

Introduction

Symbiont-bearing taxa, including corals (Hughes et al. 2018) and larger benthic foraminifera (Spezzaferri et al. 2018), can lose algal endosymbionts in a process known as "bleaching," which can be fatal (Donner et al. 2005; Hallock et al. 2006). Warming due to anthropogenic carbon emissions is associated with increased bleaching and mortality and has significantly impacted the health of coral reef communities. In the open ocean, photosymbiont-bearing planktonic foraminifera play significant roles in ecosystems and biogeochemical cycles (Schiebel 2002), but few studies have considered how photosymbiosis affects the response of species to past episodes of environmental change. This knowledge gap is important: if photosymbiont associations are particularly vulnerable, their breakdown could lead to dramatic shifts in pelagic ecosystems. In addition, planktonic foraminifera are important geochemical recorders of past global warming events, and changing photosymbiont associations could complicate the interpretation of the environmental signals they preserve.

A positive correlation between foraminiferal size and carbon isotope composition may

indicate photosymbiont activity in planktonic foraminifera (Spero and DeNiro 1987). Photosymbionts preferentially remove ^{12}C, leaving dissolved inorganic carbon (DIC) enriched in ^{13}C to be incorporated into foraminiferal tests (Spero et al. 1997). Larger specimens harbor more symbionts and therefore are relatively more enriched in ^{13}C than smaller individuals (Spero et al. 1991). Thus, photosymbiont-bearing planktonic foraminifera generally have higher $\delta^{13}C$ values (intercepts) and steeper size-specific $\delta^{13}C$ curves (slopes) than asymbiotic foraminifera. Decreases in the size-$\delta^{13}C$ slope are commonly attributed to bleaching (Wade et al. 2008; Edgar et al. 2013; Luciani et al. 2017; Si and Aubry 2018) but may be driven by other factors, such as a change in the type or number of symbionts, a change in seasonality or depth habitat of host foraminifera, or a change in the extent of gametogenic calcification (Norris 1998; Birch et al. 2013; Ezard et al. 2015).

The size-$\delta^{13}C$ relationship has been used to argue that bleaching was a contributing factor in the extinction of *Morozovelloides crassatus* in the latest middle Eocene (~38 Ma) (Wade et al. 2008) and for localized responses of photosymbiont associations in the genera *Acarinina* and *Globigerinatheka* during the middle Eocene climatic optimum (MECO, ~40 Ma) (Edgar et al. 2013). Henehan et al. (2020) provided further support for localized responses of photosymbiont associations to the MECO by finding no reduction in isotopic gradients in the south Atlantic or equatorial Pacific. Warming during the MECO amounted to only ~2°C over 100 kyr at Site 1051 (Edgar et al. 2013), and it seems questionable that such low warming rates, during the relatively cooler mid-late Eocene, would result in bleaching. Bleaching has also been invoked as a response to the even more gradual, multimillion-year warming into the early Eocene climate optimum (Luciani et al. 2017). Compounding the problem of interpreting isotopic signals are the potential effects of diagenesis (Pearson et al. 2001) and sediment mixing (Hull et al. 2011; Kirtland Turner et al. 2017; Hupp et al. 2019; Hupp and Kelly 2020), which alter the primary isotopic signal and/or its interpretation.

The relationship between warming and bleaching is complicated by the fact that photosymbiont-bearing planktonic foraminifera appear to have been more resilient to warming than asymbiotic foraminifera during the Paleocene–Eocene thermal maximum (PETM), the largest abrupt global warming event of the Cenozoic (Kelly 2002; Petrizzo 2007). Photosymbiotic taxa migrated to higher latitudes, evolved into short-lived species and morphotypes ("excursion taxa"), and increased in abundance relative to asymbiotic clades (Kelly et al. 1996; Kelly 2002; Speijer et al. 2012) in most sites. The exceptions to this generalization are a few low-latitude, neritic localities where it has been argued that exceptionally high local temperatures resulted in the total exclusion of eukaryotic plankton (Aze et al. 2014; Frieling et al. 2017). Some of these species may have also changed depth habitat and photosymbiont associations (Kelly et al. 1996; Si and Aubry 2018), affecting their isotopic composition. Interestingly, photosymbiotic scleractinian corals also appear relatively resilient (i.e., lower extinction rates) than asymbiotic species from the latest Paleocene to early/middle Eocene (Weiss and Martindale 2019), and there is no evidence for an elevated extinction across scleractinians at this time (Simpson et al. 2011). There is, however, abundant evidence for a contraction in the extent of coral–algal dominated reefs (Pandolfi and Kiessling 2014) and an expansion of encrusting foraminifera-dominated microbial reefs at this time (Plaziat and Perrin 1992; Scheibner and Speijer 2008).

Here we investigate changes in planktonic foraminiferal photosymbiont ecology across the PETM (~55.8 Ma), when sea-surface temperatures may have risen by 5°C–8°C, at low and high latitudes, respectively (Zachos et al. 2003; Dunkley Jones et al. 2013) over 2–5 kyr (Kirtland Turner et al. 2017; Kirtland Turner 2018). Many estimates of warming and carbon emissions across this event were generated using the isotope compositions of planktonic foraminifera. Deconvolving the effect of biological change on proxy-based environmental reconstructions is thus central to understanding the mechanisms and effects of the PETM. We generated new records of size-specific stable isotope compositions and relative abundance changes in three clades

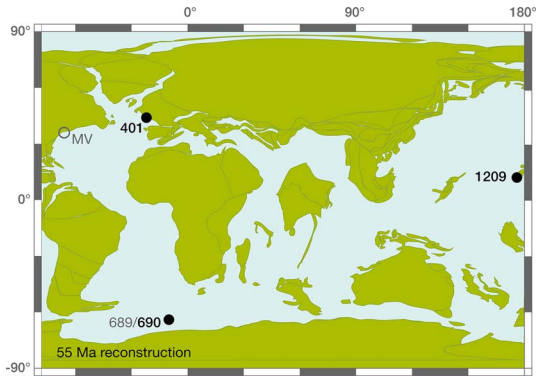

FIGURE 1. Paleogeographic map for 55 Ma (www.odsn.de; Hay et al. 1999). Sites used in analyses indicated by black circles; other sites cited in the text indicated by gray circles.

of planktonic foraminifera from three ocean drilling sites (Sites 1209, 401, and 690) (Fig. 1) and considered these along with size-specific isotope records from Millville, NJ (Si and Aubry 2018).

Materials and Methods

Site Locations and Depths.—Data are presented from seven time slices at ODP Site 1209 (Central Pacific, paleolatitude = ~24°N), five time slices at DSDP Site 401 (midlatitude North Atlantic, paleolatitude = ~43°N), and seven time slices at ODP Site 690 (Southern Ocean, paleolatitude = ~66°S), spanning the PETM (Fig. 1, Supplementary Tables 1–6; paleodepths of all sites = 1900–2000 m during the PETM) (Winguth et al. 2012). We compared our data with those from Millville on the New Jersey shelf (ODP Leg 174X) (Si and Aubry 2018), at a paleolatitude of 35°N (Kopp et al. 2009) and a paleodepth of ~70–150 m (Sugarman et al. 2005; Stassen et al. 2014).

Methods.—We measured stable carbon and oxygen isotopes of planktonic foraminiferal tests across the PETM in samples from Sites 401, 690, and 1209 sorted by size. Samples from Site 1209 were sieved into 6 size fractions (150–425 μm), from Site 401 into 10 size fractions (75 to >425 μm), and from Site 690 into 7 size fractions (125 to >355 μm) (Supplementary Table 1). Different size fractions were used at each site as data were collected by separate research groups and initially intended for different studies. We refer to size fractions by their smaller sieve-size boundary, that is, "150" refers to 150–180 μm. In each size fraction, we aimed to measure 30 individuals per taxon (as an averaged, homogenized sample).

Photosymbiont-bearing and non-photosymbiont-bearing planktonic foraminiferal species in three clades (*Acarinina*, *Morozovella*, and *Subbotina*) were targeted (see Supplementary Table 1 for breakdown of species; Supplementary Figs. 5–6). These three genera are by far the most common planktonic genera in early Paleogene assemblages (Kelly 2002; Petrizzo 2007; Figs. 2–4). *Acarinina* and *Morozovella* have size-$\delta^{13}C$ trends and oxygen isotope–inferred habitat depths indicative of photosymbiont-bearing, mixed-layer life histories (Pearson et al. 2006). Carbon and oxygen isotope ratios in *Subbotina*, by contrast, suggest an asymbiotic, thermocline-dwelling life history (D'Hondt et al. 1994). Deep-sea (asymbiotic) epifaunal foraminifera (*Nuttallides truempyi*) were also measured at Site 1209 for comparison with preexisting measurements from the same species at Sites 401 and 690 (references in Figs. 2–4). Site 1209 specimens were photographed before isotopic analysis (Supplementary Table 3), and preservation was examined using scanning electron microscopy (SEM) (Supplementary Fig. 1).

Isotopic analyses were performed at Yale University, the University of California, San Diego, and the University of California, Santa Cruz (see Supplementary Material). At Site 401, we generated genus-level assemblage counts by identifying ~360 individuals in splits of the >125 μm size fraction in 48 samples across Core 14 for comparison with published data for Sites 1209 (Petrizzo 2007) and 690 (Kelly 2002). Comparable counts are not available for Millville.

We assessed changes in photosymbiont status using terms agnostic to the potential driver of the signal. "Isotopic shallowing" describes a decrease in size-$\delta^{13}C$ gradients consistent with reduced photosynthetic activity, perhaps to the point of total loss (bleaching). "Isotopic steepening" refers to increased size-$\delta^{13}C$ gradients consistent with enhanced photosynthetic activity. We quantified size-$\delta^{13}C$ relationships using linear regressions. For Sites 1209, 401,

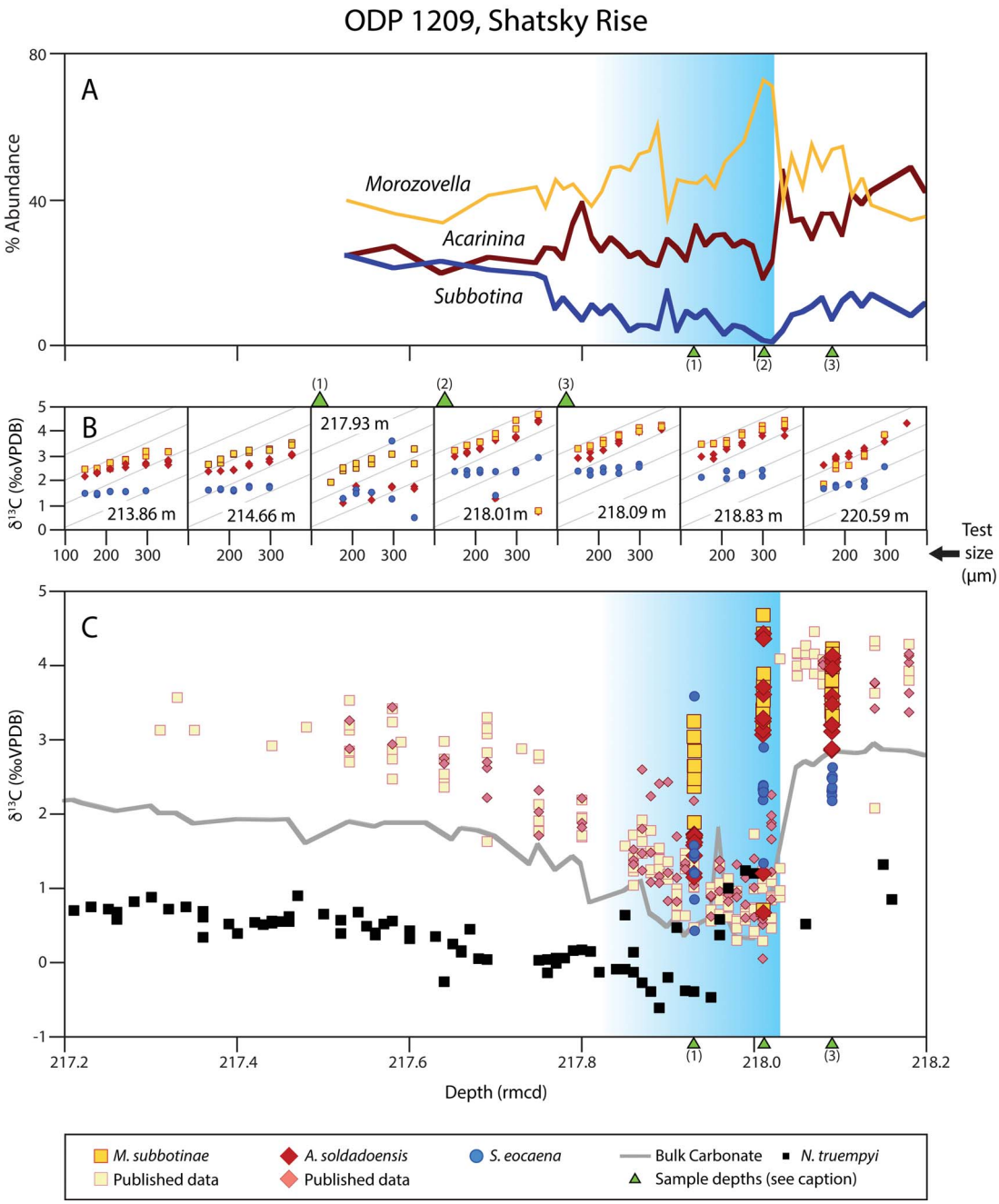

FIGURE 2. Abundance and isotopic data for foraminifera from ODP Site 1209. Blue background shading indicates onset of the Paleocene–Eocene thermal maximum (PETM). A, Percent abundance of *Acarinina*, *Morozovella*, and *Subbotina* (Petrizzo 2007). B, Time slice–specific size-$\delta^{13}C$ of planktonic foraminifera, with sample placement indicated by green triangles in A and C, if within the plotted depth range. Gray inset lines indicate maximum size-$\delta^{13}C$ slope (same across all panels). C, Published foraminiferal and bulk carbonate $\delta^{13}C$ data (Zachos et al. 2003; Dutton et al. 2005; Tripati and Elderfield 2005; Takeda and Kaiho 2007; Westerhold et al. 2011; Gibbs et al. 2012; Penman et al. 2014). Blue gradient indicates onset of the PETM. rmcd, revised meters composite depth.

and 690, insignificant slopes were generally caused by a lack of size-$\delta^{13}C$ trend (i.e., slopes approaching zero). For samples from Millville, isotopic data in each time bin were limited, and insignificant slopes were caused by slopes approaching zero and small sample sizes.

We examined changes in the difference in the $\delta^{13}C$ and $\delta^{18}O$ of individuals in the 150–212 μm sieve fractions (the smallest analyzed across all three sites) between planktonic and benthic foraminifera in order to consider shifts in the basal isotopes relative to deep-ocean values. These comparisons use a "Δδ" notation (e.g., $\Delta\delta^{13}C_{Acarinina\text{-}Benthic}$). This allowed us to compare relative changes in photosymbiont-bearing and asymbiotic clades and to consider changes in depth habitat and ecology.

Results

We generated 394 size-specific planktonic foraminiferal isotopic measurements from Sites 1209 (Central Pacific), 401 (midlatitude North Atlantic), and 690 (Southern Ocean) (Supplementary Table 5; Supplementary Fig. 2); 16 benthic isotopic measurements from Site 1209 (Supplementary Table 6); and assemblage counts from 48 samples at Site 401. To distinguish between patterns inferred from individual samples and from aggregated samples, we use the terms "time slice" and "time bins," respectively. The PETM has a characteristic carbon isotope stratigraphy that can be used to divide it into time bins for the comparison of changes across sites (Figs. 2–4, Supplementary Table 4). This includes a geologically abrupt negative carbon isotope excursion (CIE) of ~2‰–3‰ in carbonates at the start of the event, a sustained nadir lasting ~50 kyr (i.e., the body of the CIE), followed by ~150 kyr recovery to pre-event–like carbon isotope values. Here we use a "pre-PETM" time bin for all samples before the negative CIE of the PETM and a "core-PETM" time bin for samples in the body of the CIE. At ODP Site 690, where we have multiple samples in the body of the CIE, we discuss our three CIE samples in two time bins (earliest CIE sample = "base-PETM," two later CIE samples = core-PETM; Supplementary Table 4), as they differed markedly in stable isotopic patterns and values (attributed to size-dependent mixing; Hull et al. 2011; Kirtland Turner et al. 2017; Hupp et al. 2019; Hupp and Kelly 2020). Here, acarininids and subbotinids have nearly identical $\delta^{13}C$ values in the base-PETM sample, but distinct values in the core-PETM samples. We use the term "post-PETM" to indicate samples above the core CIE. At Site 1209, post-PETM includes samples from well above the $\delta^{13}C$-recovery interval (Fig. 2). At Site 401, post-PETM includes samples from both the $\delta^{13}C$-recovery and postrecovery intervals. At Site 690 post-PETM includes samples from the $\delta^{13}C$-recovery alone. In all sites, by the post-PETM interval, $\delta^{13}C$ increases rapidly with size in photosymbiotic species.

Foraminifera–Symbiont Relations.—Across all sites and most time slices, $\delta^{13}C$ of *Acarinina* and *Morozovella* species increases with size (Figs. 2–4, Supplementary Tables 7–8), consistent with extant foraminifera externally hosting photosymbionts (D'Hondt et al. 1994; Gaskell and Hull 2019) (Supplementary Figs. 2–7). In contrast, *Subbotina* only rarely shows a significant size-$\delta^{13}C$ trend, consistent with an asymbiotic life history (D'Hondt et al. 1994). The size-$\delta^{13}C$ relationships of *Acarinina* and *Morozovella* vary within sites among samples and among sites. On average, size-$\delta^{13}C$ slopes of the photosymbiotic species are the steepest at midlatitude Atlantic Site 401 (Fig. 3) and shallowest at central Pacific Site 1209 (Fig. 2). At Southern Ocean Sites 690 and 689 (Si and Aubry 2018), regression slopes were insignificant in the pre-PETM records for photosymbiotic species due to the near absence of size-$\delta^{13}C$ enrichment.

Isotopic Responses to the PETM by Site.—At Site 1209, size-$\delta^{13}C$ gradients of *Acarinina* and *Morozovella* vary as much (or more) between time slices outside the PETM as between time slices within and outside the PETM (Fig. 2, Supplementary Figs. 8–9). Size-$\delta^{13}C$ gradients were slightly reduced in the PETM relative to pre-event, and responses vary by photosymbiotic clades above the PETM. The isotopic values of planktonic foraminifera in the earliest core-PETM sample (218.01 revised meters composite depth [rmcd]) match pre-PETM values, likely due to the displacement of material up-section during prior core sampling. One of

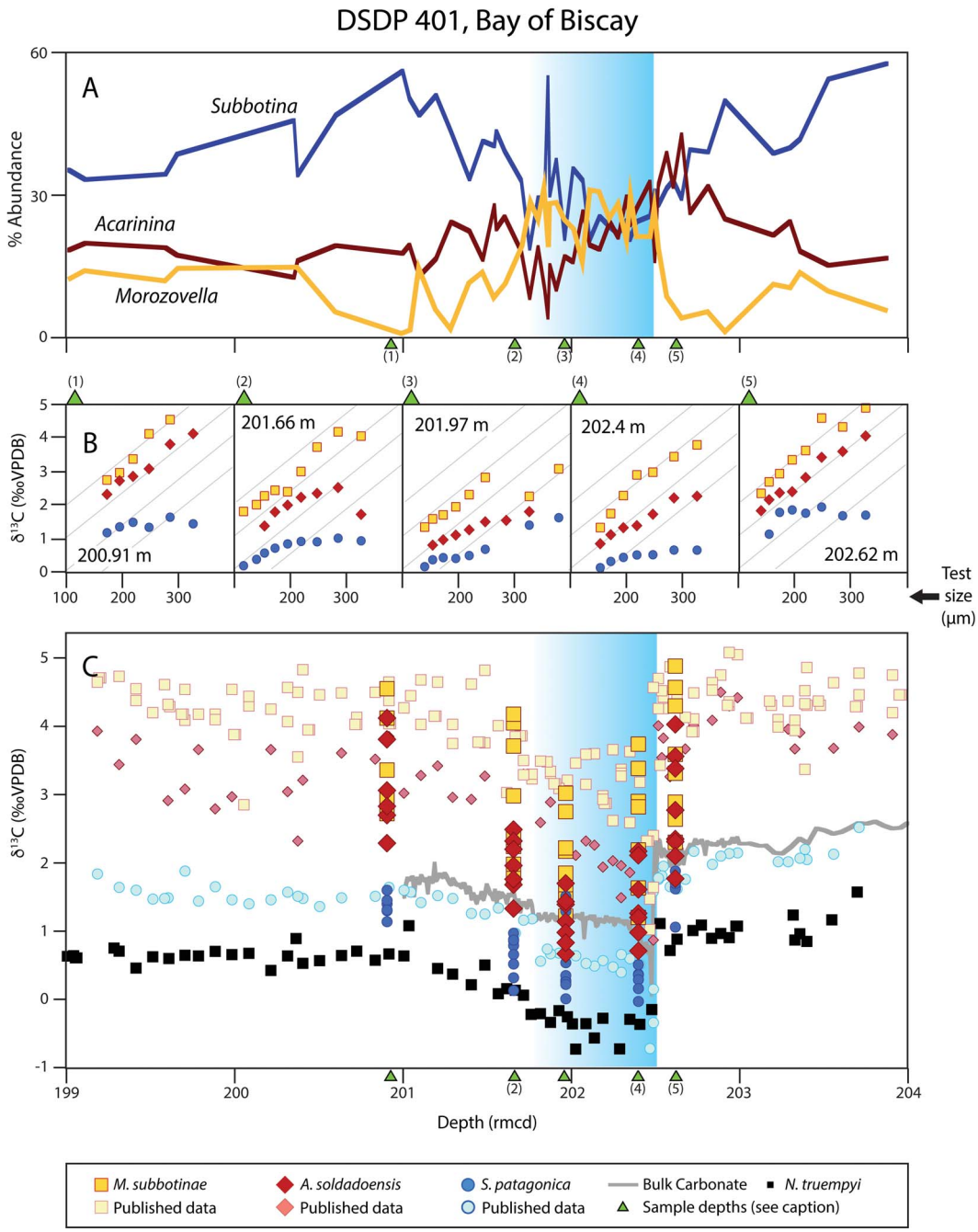

FIGURE 3. Abundance and isotopic data for foraminifera from DSDP Site 401. Blue background shading indicates onset of the Paleocene–Eocene thermal maximum (PETM). A, Percent abundance of *Acarinina*, *Morozovella*, and *Subbotina*. B, Time slice–specific size-$\delta^{13}C$ of planktonic foraminifera, with sample placement indicated by green triangles in A and C, if within the plotted depth range. Gray inset lines indicate maximum size-$\delta^{13}C$ slope (same across all panels). C, Published foraminiferal and bulk carbonate $\delta^{13}C$ data (Pardo et al. 1997; Katz et al. 2003; Nunes and Norris 2006; D'Haenens et al. 2012; Bornemann et al. 2014, 2016; Gutjahr et al. 2017). rmcd, revised meters composite depth.

the authors (E.T.) took this sample and observed extensive core depletion and disruption. We assume that disruption and displacement explain the pre-PETM–like values

(Fig. 2B) relative to findings in other studies for the same time interval (Fig. 2C), and we exclude this sample from further discussion. The second core-PETM sample (217.93 rmcd) is considered in place, as isotopic values for *Acarinina* match those of previous studies in the same size class (compare Fig. 2B and C) and the average $\delta^{13}C$ values of subbotinids and morozovellids decline by >1‰ relative to pre-PETM $\delta^{13}C$ values. In the core-PETM (Fig. 2B), acarininids are lower in $\delta^{13}C$ than before the PETM onset, with values similar to subbotinids (Supplementary Fig. 10, Supplementary Table 9) and relatively flattened size-$\delta^{13}C$ slopes. Moderate to poor preservation may account for some of the record (Fig. 2, Supplementary Fig. 4) including (1) inverted morozovellid and acarininid $\delta^{18}O$ values relative to other sites, (2) low size-$\delta^{13}C$ gradients, (3) modest differences in isotopic values among species, and (4) a minimum in the $\delta^{18}O$ and $\delta^{13}C$ difference between benthic and planktonic clades during the PETM (Supplementary Fig. 13). However, the consistency of preservation across samples suggests that it did not influence size-$\delta^{13}C$ relationships over time (SEM images, Supplementary Fig. 1).

Before the PETM, morozovellids and acarininids had similar abundances at Site 1209, each comprising 30%–50% of the assemblage. Within the PETM, morozovellid abundance increased rapidly, with a peak abundance of >70% in the core PETM, due to an increase in the relative abundance of *M. velascoensis* (up to 40%), a decline in acaraninids, and an absence of subbotinids (Fig. 2).

At Site 401, positive size-$\delta^{13}C$ relationships occur in *Acarinina* and *Morozovella* throughout all time slices (Fig. 3), but gradients decrease within the PETM. The size-$\delta^{13}C$ slopes of both clades continue to decrease in the second core-PETM sample (Fig. 3, Supplementary Table 8). Gradients then increase through post-PETM time slices, eventually reaching pre-PETM values. The difference in $\delta^{18}O$ between benthic foraminifera and planktonic clades varies over the record, with a minimum $\delta^{18}O$ gradient within the PETM (Supplementary Fig. 10, Supplementary Table 9). The maximum difference in $\delta^{18}O$ between benthic and planktonic clades occurs above the PETM. From pre- to post-PETM, $\Delta\delta^{13}C_{Benthic}$ increased ~0.5‰ in *Acarinina*, decreased by 0.5‰ in *Subbotina*, and changed little in *Morozovella*. Subbotinids make up 40%–70% of assemblages before the PETM at Site 401 but fall to ~30% within the core-PETM. Within the PETM, morozovellids increased distinctly in relative abundance (from ~10% to ~30%), coincident with the pronounced decrease in the relative abundance of subbotinids and acarininids (Fig. 3).

At Site 690, all pre-PETM time slices indicate insignificant size-$\delta^{13}C$ slopes in *Acarinina* (Fig. 4). Two species of *Acarinina* (*A. soldadoensis* and *A. coalingensis*) and *Subbotina* (*S. patagonica* and *S. triangularis*) were analyzed but have minimal differences in isotopic signatures (Supplementary Fig. 11), so results are considered at the genus level. Morozovellids are extremely rare outside the core-CIE at Site 690 and are thus not considered (Kelly 2002). *Acarinina* had an insignificant size-$\delta^{13}C$ relationship in the onset of the PETM (−0.326 ‰/100 µm; Fig. 4, depth 170.48 m), and $\delta^{13}C$ values collapse onto those of *Subbotina* (Supplementary Fig. 10). Size-$\delta^{13}C$ gradients of *Acarinina* increase markedly from the base- to the core-PETM and post-PETM, reaching slopes comparable to those at Site 401 (Fig. 4, Supplementary Table 7). The relative abundance of subbotinids fell by half at the CIE initiation, coincident with an increase in acarininids (i.e., the "acarininid spike"; Kelly 2002), with variation in the relative abundance of both clades thereafter. The base of the PETM coincides with an inversion in the $\Delta\delta_{Planktonic\text{-}Benthic}$ of $\delta^{13}C$, with $\delta^{18}O$ inverting in the core-PETM interval (Supplementary Fig. 13).

Time slices at the Millville site are sparsely sampled, leading us to group samples over 20 −180 cm (Supplementary Fig. 7; as in Si and Aubry 2018). Below the PETM, $\delta^{13}C$ values are comparable to Site 401 pre-PETM for all three clades (Supplementary Fig. 7), but values collapse by ~2‰ at the PETM, and do not fully recover over the studied record. The size-$\delta^{13}C$ slope of *Acarinina* decreased from the pre-PETM (positive but insignificant regression coefficients) to the core-PETM (Supplementary Fig. 7), but the Paleocene time slice contains only four data points for *Acarinina* and three for *Morozovella* and is thus hard to evaluate.

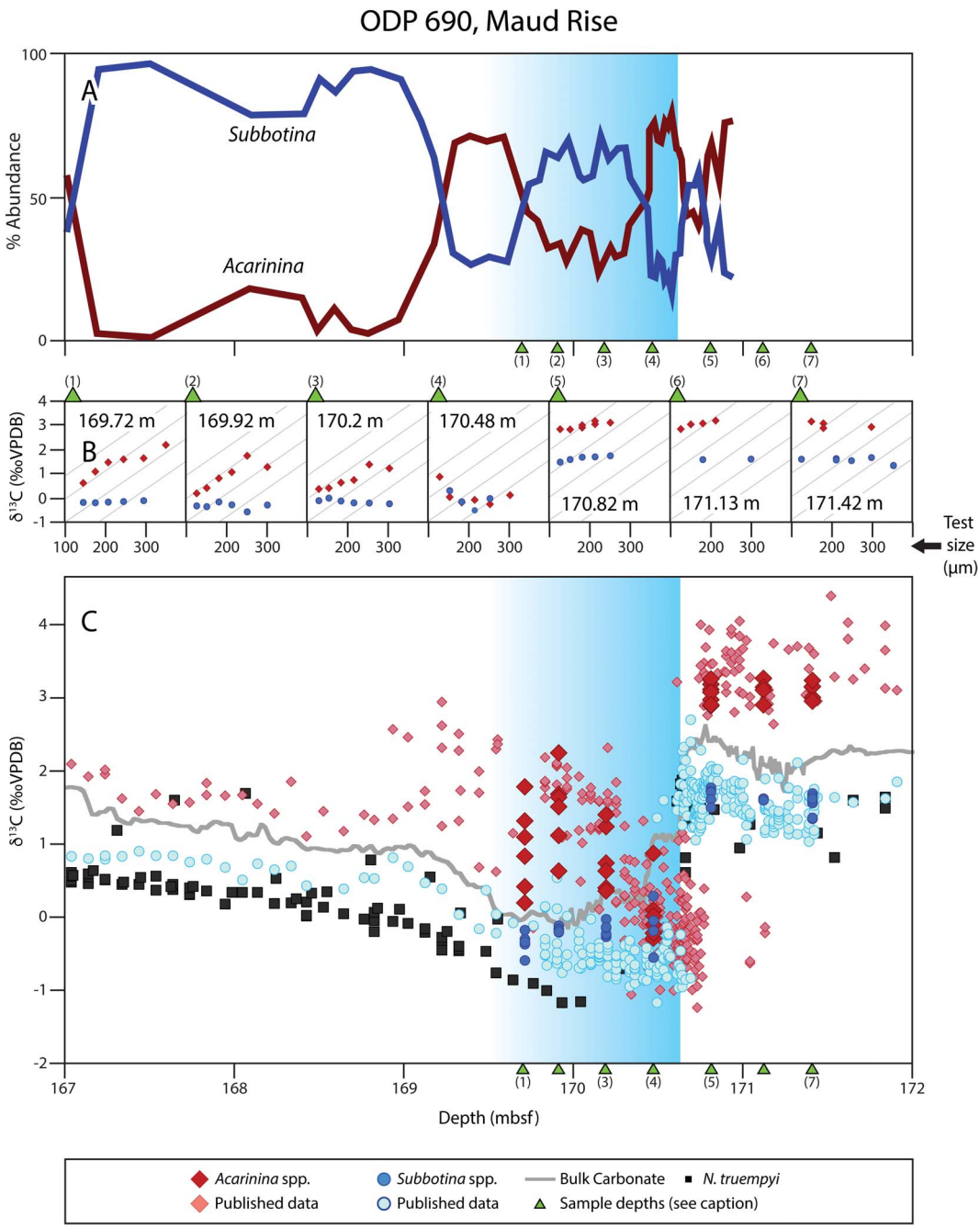

FIGURE 4. Abundance and isotopic data for foraminifera from ODP Site 690. Blue background shading indicates onset of the Paleocene–Eocene thermal maximum (PETM). A, Percent abundance of *Acarinina* and *Subbotina* (Kelly 2002). B, Time slice–specific size-$\delta^{13}C$ of planktonic foraminifera, with sample placement indicated by green triangles in A and C, if within the plotted depth range. Gray inset lines indicate maximum size-$\delta^{13}C$ slope (same across all panels). C, Published foraminiferal and bulk carbonate $\delta^{13}C$ data (Kennett and Stott 1991; Thomas and Shackleton 1996; Bains et al. 1999; Thomas et al. 2000, 2002; Cramer et al. 2003; Kelly et al. 2005, 2012). rmcd, revised meters composite depth.

The shallowest size-$\delta^{13}C$ slopes for *Acarinina* and *Morozovella* occur in the youngest sample in the late recovery from the event (Supplementary Fig. 7). $\Delta\delta_{Planktonic\text{-}Benthic}$ cannot be readily

compared with our data, as different benthic species were measured at Millville (*Cibicidoides* spp. in the pre-PETM, and *Anomalinoides acuta* in the PETM and post-PETM, as compared with *Nuttallides truempyi*) (Supplementary Fig. 10).

Discussion

We looked for evidence of changes in photosymbiont associations, including evidence of bleaching, in foraminifera across the most prominent hyperthermal of the Cenozoic (i.e., the PETM), using size-$\delta^{13}C$ trends as a proxy for the presence and strength of photosymbiont associations. At midlatitude North Atlantic Site 401 and Central Pacific Site 1209, size-$\delta^{13}C$ enrichment was reduced during the PETM (i.e., isotopic shallowing) for photosymbiont-bearing taxa, consistent with a reduction in photosymbiont activity (Figs. 2, 3), an effect that was more pronounced in acarininids than morozovellids. At Site 401, our planktonic foraminiferal isotope records are consistent with published $\delta^{13}C$ values in the same size class across the event (Fig. 3C), but this is not the case for the core-PETM samples at Site 1209. We have one sample at Site 1209 (217.93 rmcd) capturing the core-PETM interval, but our carbon isotope values for *Morozovella subbotinae* are higher than published measurements of *M. velascoensis* (Fig. 2C). Both *M. subbotinae* and *M. velascoensis* yield similar $\delta^{13}C$ values pre-PETM (~0.2‰–1‰; Fig. 2C), but during the core-PETM (217.93 rmcd), *M. velascoensis* has values of 1‰–1.2‰ and *M. subbotinae* has values of 2‰–3‰. These two species also respond differently to the event in terms of relative abundance: the abundance of *M. velascoensis* (the species with the greatest decrease in $\delta^{13}C$) increases dramatically in the core-CIE to account for nearly 40% of all individuals sampled, while *M. subbotinae* maintained similar relative abundances (or even declined slightly) (Petrizzo 2007). All isotopic data for *Acarinina* at Site 1209 are from a single species, *A. soldadoensis*, and our isotopic values for *Acarinina* are consistent with published acarininid data (Fig. 2).

Isotopic shallowing with the onset of the PETM is not consistent across sites. The Southern Ocean record at Site 690 displays insignificant but weakly positive size-$\delta^{13}C$ slopes in acarininids in the pre-PETM interval (Fig. 4). Similarly weak isotopic enrichments are recorded in pre-PETM *A. subsphaerica* at Site 690 (Hupp et al. 2019; Hupp and Kelly 2020) and in pre-PETM acarininids from ODP Site 689 (Si and Aubry 2018). Across all Southern Ocean studies, *Acarinina* shows no significant size-$\delta^{13}C$ relationship in the middle of the core-PETM, during which *Acarinina* $\delta^{13}C$ values collapse onto those of co-occurring *Subbotina*. Both trends are captured by the record of Hupp et al. (2019) and Hupp and Kelly (2020), which have greater temporal resolution around the onset of the PETM. The shape of the acarininid collapse (occurring in the largest size fraction first and resulting in a strongly negative size-$\delta^{13}C$ relationship during the collapse) emphasizes the importance of sediment mixing and population abundance in structuring the perception of biological change (Kirtland Turner et al. 2017; Hupp and Kelly 2020). Hupp et al. (2019) and Hupp and Kelly (2020) argue that changes in the observed size-$\delta^{13}C$ relationships at Site 690 result from mixing different size classes of pre-PETM and core-PETM samples to a different degree (i.e., small size fractions mix further than large size fractions; Bard 2001); an effect potentially exacerbated by combining differential abundance changes of individuals by species and size (Thomas 2003; Kirtland Turner et al. 2017). We agree that there is pervasive evidence for an onset interval with strong sediment mixing at Sites 689 and 690 (Kelly et al. 2012; Kirtland Turner et al. 2017; Hupp et al. 2019). Although we initially thought it likely that the collapsed offset between *Acarinina* and *Subbotina* was robust to the effects of mixing, given the modeled relative abundance changes of the two clades and isotopic composition (Kirtland Turner et al. 2017: fig. 5) by 170.48 m below seafloor (our lowermost Site 690 core-PETM sample; Fig. 4), recent work by Hupp and Kelly (2020) showed evidence for mixing-related biases more than 20 cm above the CIE onset, as could also have been argued from the records in Thomas et al. (2002).

In Sites 689 and 690, strongly positive size-$\delta^{13}C$ relationships in *Acarinina* only develop

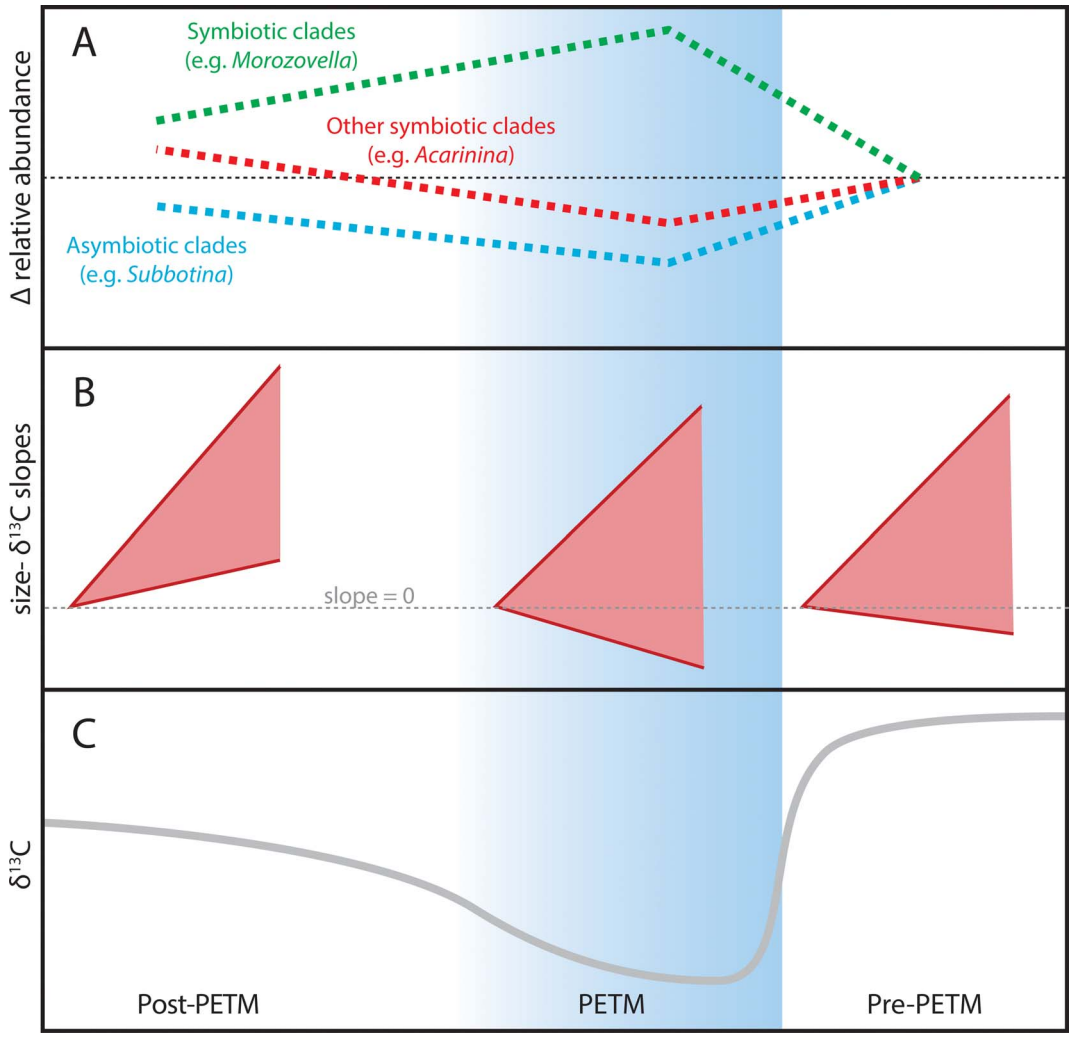

FIGURE 5. Schematic summarizing major results of this study. A, Change in relative abundance of planktonic clades as compared with pre-PETM (Paleocene–Eocene thermal maximum) values (indicated by black dashed line). Asymbiotic clades respond similarly across the PETM, decreasing in abundance during the peak of the event, whereas symbiotic clades show site- and clade-specific variation in response. B, Range of size-$\delta^{13}C$ slopes of symbiotic clades (raw slope coefficients shown in Supplementary Fig. S8) with dashed line indicating slope coefficients of 0. Symbiotic clades show a wide range of size-$\delta^{13}C$ slopes before, during, and after the PETM. C, Idealized $\delta^{13}C$ curve.

in the later part of the core-PETM. These results are consistent with weak to no photosymbiont fractionation in acarininids before the PETM and during the initial onset of the event, followed by stronger photosymbiont-mediated fractionation during the initial recovery from the PETM. Strong size-$\delta^{13}C$ enrichment in modern foraminifera with externally hosted symbionts result from increasing photosymbiont density, with test size increasing the geochemical modification of the individual's microenvironment (Spero et al. 1991; Zeebe et al. 1999; Gaskell and Hull 2019). Hence, it is plausible that symbiont ecology changed in the aftermath of the PETM. In the pre-PETM interval, acarininids (a clade typically hosting photosymbionts) may not have increased their photosymbiont population sufficiently to drive an increasing microenvironment effect, whereas in the later parts of the core-PETM they may have done so. All open-ocean sites considered in this study show isotopic steepening in

photosymbiotic taxa in the later stages of the PETM relative to the core-PETM, with *Acarinina* gaining significant size-$\delta^{13}C$ enrichment for the first time in the Southern Ocean in the post-PETM interval (Fig. 4). In addition, the Southern Ocean collapse in $\delta^{13}C$ at the onset of the PETM could reflect a change in relative depth habitat, as argued by Si and Aubry (2018), as the $\delta^{18}O$ gradient collapsed simultaneously (as in Millville) (Supplementary Fig. 10). A minimum in the difference in $\delta^{18}O$ between benthic foraminifera and planktonic clades during the CIE is observed at Site 401 and could also have been driven by a change in depth habitat (Supplementary Fig. 10, Supplementary Table 9). However, collapsed offsets are also expected due to differential mixing by species, abundance change, and size class (Kirtland Turner et al. 2017; Hupp et al. 2019; Hupp and Kelly 2020), and these may simply reflect the effect of well-documented mixing artifacts.

The shelf record from Millville (Si and Aubry 2018) displays no clear evidence for isotopic shallowing in morozovellids or acarininids during the PETM, consistent with the inference that coastal foraminifera did not experience the loss of photosymbiont-mediated fractionation, compared with open-ocean sites. Alternatively, the absence of a clear signal may reflect the high variance in the data and the need to group samples to achieve interpretable records.

Evidence for isotopic shallowing and steepening raises the question whether changes are driven by photosymbiont loss and gain, respectively. In extant corals, "bleaching" refers to total photosymbiont loss, but many factors, biological and environmental, could drive changes in size-$\delta^{13}C$ gradients in planktonic foraminifera, without total photosymbiont loss. Isotopic shallowing could be driven by (1) partial or complete loss of symbionts, (2) reduction in photosymbiont density, (3) reduction in photosymbiont metabolism (e.g., due to changes in irradiance or temperature), or (4) a switch to a different clade of symbionts. Corals (Santavy et al. 2005) and benthic foraminifera (Schmidt et al. 2018) show such changes and can experience partial bleaching ("paling") rather than total photosymbiont loss.

The weak and variable evidence for size-$\delta^{13}C$ gradients at high-latitude Sites 689 (Si and Aubry 2018; Supplementary Fig. 12) and 690 (Fig. 4) before the PETM suggests that *Acarinina* varied its relationships with photosymbionts in response to local conditions. Such variation in host–photosymbiont relationships and their isotopic expression is known in extant planktonic foraminifera, which vary in the density (Bird et al. 2017; Takagi et al. 2018, 2019) and type of photosymbionts (Schiebel and Hemleben 2017; Takagi et al. 2019), location where symbionts are hosted (i.e., intra- vs. extracellularly) (Spero 1998; Bird et al. 2017; Schiebel and Hemleben 2017), and degree to which photosymbiosis is reflected in size-$\delta^{13}C$ enrichment (Ezard et al. 2015; Edgar et al. 2017).

Differences in the persistence and magnitude of $\delta^{13}C$ change between morozovellids and acarininids, and between two different species of morozovellids at Site 1209, indicate species-specific differences in photosymbiont associations. Complete loss of size-$\delta^{13}C$ enrichment occurs within *Acarinina soldadoensis* in a single time slice only (Fig. 2B, 217.93 rmcd), although post-PETM samples have reduced size-$\delta^{13}C$ gradients throughout the length of our record. We see a similar absence of size-$\delta^{13}C$ relationship at the onset of the PETM in Site 690 (Fig. 4). In both cases, the lack of a size-$\delta^{13}C$ gradient in the base-/core-PETM is consistent with a different foraminifera–photosymbiont relationship than is typical of acarininids, such as the loss of symbionts or reconfiguration of the relationship. This may have involved photosymbiont clades with small fractionation effects in $\delta^{13}C$ or moving symbionts internally to the test where they have smaller microenvironmental (and thus isotopic) effects. In midlatitude Site 401 (Fig. 3B), acarininids show distinct isotopic shallowing during the PETM, consistent with a changed foraminifera–photosymbiont association, but morozovellids do not, at least in small- to medium-sized individuals. It is common for the largest individuals of photosymbiont-bearing species to show weaker size-$\delta^{13}C$ fractionation effects than smaller individuals, which is attributed to ontogenetic effects such as gametogenic calcification, which could account for differences among size fractions. Hupp et al. (2019) and Hupp and Kelly (2020) proposed a similar pattern during the onset of the PETM at Site 690 to

be a preservational artifact of differential mixing depths and abundance changes across size fractions, an explanation that works equally well to explain the disconnect in isotopic changes across size fractions at Site 401, but not the differential response of acarininids and morozovellids to the PETM.

Although environmental and preservational changes are important drivers of isotopic variation in fossil foraminifera, they are not likely to be the primary cause of the major patterns we observe. Preservation can dramatically alter the isotopic signals preserved (Pearson et al. 2001), but the sites with the best (Site 401) and worst (Site 1209) preservation have the most similar patterns of isotopic change across the PETM (Figs. 2,3, Supplementary Material). Environmental differences offer an alternative explanation for variable isotopic patterns among sites, including factors such as the availability of photosynthetically active radiation, temperature, carbonate ion effects, and the extent of water-column stratification (Spero et al. 1997; Lombard et al. 2009; Henehan et al. 2016). This class of explanations is less parsimonious than those invoking changed photosymbiont associations, because variable combinations of environmental changes need to be evoked at each site (Supplementary Table 2). For instance, at Site 401 the two photosymbiont-bearing clades show different PETM responses, whereas at Site 1209 these clades show identical responses. To account for this via the environment, a variable combination of temperature, depth, and stratification changes are needed to explain divergent isotopic patterns in co-occurring photosymbiotic clades. Similarly, the combined effects of sediment mixing and relative abundance changes (as in Hupp et al. 2019; Hupp and Kelly 2020) do not provide a straightforward explanation, as there are divergent relative abundance pattern changes across acarininids and morozovellids at Sites 401 and 1209, and these factors require follow-up mixing studies to fully address.

At present, we favor the relatively parsimonious explanation of variation in the strength (or location) of photosymbiont associations as the most probable mechanism responsible for observed isotopic shallowing and steepening across the PETM. The lack of size-$\delta^{13}C$ relationships during the PETM in some species and sites likely does not indicate symbiont bleaching. Rather, we hypothesize that the importance of photosymbiont associations to the metabolic functions of individual foraminifera can vary in response to conditions experienced during a life span, resulting in variation in the isotopic expression of photosymbiosis. Our approach obviates the need to explain how and why bleaching would occur for tens to hundreds of thousands of generations in response to relatively minor temperature changes. Photosymbiotic associations in some shallow-water living benthic foraminifera are variable and have high thermal tolerances (Schmidt et al. 2016, 2018), and microevolutionary responses such as the adoption of more thermally resistant photosymbionts or sustained photoinhibition (Rowan 2004) could occur over the kiloyear-long onset of the PETM (Dunkley Jones et al. 2013; Kirtland Turner et al. 2017), making complete bleaching a less likely explanation.

Given evidence presented here for widespread changes in photosymbiont associations, it is remarkable that populations of photosymbiont-bearing clades apparently thrived relative to asymbiotic clades during the PETM. At low latitudes, *Morozovella* peaked in relative abundance during the PETM, and in high latitudes, *Acarinina* also increased in abundance (Figs. 2–4), possibly responding to increasingly oligotrophic conditions in the water column (Bralower 2002). Remarkably, we find that the morozovellid species with the greatest $\delta^{13}C$ reductions (*M. velascoensis*) at Site 1209 does extremely well, from a population abundance perspective, during the PETM (Fig. 2), increasing in relative abundance to ~40% of the total population (Petrizzo 2007). On the other hand, acarininids, which saw the complete elimination of size-$\delta^{13}C$ fractionation, fell in abundance from ~40% before the PETM to ~30% during the PETM. Further evidence for adaptive responses comes from the collapse in $\delta^{18}O$ offsets between surface and mixed-layer taxa at Millville and in the Southern Ocean, attributed to changes in depth habitat or seasonality (Stap et al. 2010; Si and Aubry 2018). The combined isotopic and abundance data present a compelling case for the relative resilience of photosymbiont-bearing planktonic

foraminiferal clades to PETM environmental changes as compared with asymbiotic clades.

Possibly, the rate of climate change during the PETM (roughly an order of magnitude slower than today; Kirtland Turner 2018), enabled flexible planktonic foraminifera–photosymbiont associations, allowing populations of some species to thrive. In other words, photosymbiont bearers might not be particularly vulnerable to all global change events, but just to those that cause complete loss of symbionts on very short timescales (a few generations), as observed today. However, if PETM warming included extreme, short-term climatic events superimposed on longer-term warming trends, with rates of change more analogous to today, our results might simply indicate that photosymbiotic planktonic foraminifera are more resilient than the better-studied symbiotic corals and larger benthic foraminifera today (Hughes et al. 2018; Prazeres 2018; Spezzaferri et al. 2018). Alternatively, ancient photosymbiotic associations in much warmer climate states may have been more resilient to warming than those observed in the much cooler oceans of the late Cenozoic (Stanley and van de Schootbrugge 2018).

Regardless of the ultimate driver, planktonic foraminiferal isotopic changes across the PETM demonstrate the importance of establishing site-specific baselines for environmental interpretations of geochemistry across the PETM. Depth habitat and photosymbiont activity, both of which changed during the PETM, influence the isotope composition of foraminiferal tests, perhaps accounting for some variation in CIE magnitude estimates (i.e., 2‰ and 7‰; Kennett and Stott 1991; Sluijs and Dickens 2012). In addition, the spatial and depth distribution of CIEs, and their relative magnitude, have been used to constrain the source and timing of PETM carbon emissions (Kirtland Turner 2018). A spatially variable response of photosymbiosis complicates inferences, because it decouples changes in $\delta^{13}C_{calcite}$ from changes in $\delta^{13}C_{DIC}$, with the magnitude and pattern of changes in $\delta^{13}C_{DIC}$ needed to make inferences regarding carbon release. Changes in photosymbiosis and depth habitat across the PETM would also affect the magnitude of boron isotope change measured, an important proxy of ocean pH and atmospheric pCO_2 (Penman et al. 2014; Gutjahr et al. 2017).

Conclusions

Changes in physiology, ecology, and photosymbiont status can profoundly alter geochemical records. Photosymbiont-bearing foraminifera provide key records of atmospheric CO_2 and surface ocean temperatures, and their ecologies are central to making accurate environmental reconstructions via geochemical analyses. Isotopic shallowing during the PETM thus may obscure the environmental signal of the event and, when unaccounted for, will result in erroneous environmental reconstructions from $\delta^{13}C$- and $\delta^{11}B$-based proxies.

Ancient global environmental perturbations provide case studies in biotic response over long ecological and evolutionary timescales. Today, warming-induced bleaching elevates mortality rates of some photosymbiont-bearing taxa, contributing to the collapse of populations in critical groups, including corals. Whether photosymbiont-bearing species can adapt via microevolutionary responses in the long term is a major question that is difficult to answer on the timescales of modern ecological studies. Our results from the fossil record provide important constraints and suggest that the adaptative capacity of photosymbiotic species may be so great as to allow some populations to expand, and excursion species to evolve, during relatively protracted climate change relative to the generation time of the species (i.e., warming over kiloyears). Historical archives should be considered alongside modern ecological studies (e.g., Hughes et al. 2018; Prazeres 2018; Spezzaferri et al. 2018) to consider how multigenerational evolutionary responses can mitigate the physiological stress of environmental perturbations.

We show evidence of spatially variable, changing photosymbiont associations in planktonic foraminifera in response to the PETM, rather than homogenous bleaching-like signals, which suggests site- and time-specific investigations are needed before isotopic records can be interpreted confidently with regard to environmental conditions and the biasing effects of sediment mixing and variable diagenesis

(Fig. 5). Our results are consistent with the spatially variable impacts of the PETM. Modern coral bleaching is not globally uniform due to local environmental conditions, clade-specific symbiont associations, and clade-specific adaptations. We should expect—as we, in fact, observe—similar variability in foraminifera–photosymbiont associations in the past.

As to understanding the physiological and ecological response of taxa to global warming, we show that populations of photosymbiotic species were resilient to relatively gradual global warming during the PETM. Photosymbiont-bearing planktonic foraminifera were relatively more abundant than asymbiotic clades after the onset of the PETM at most sites. Symbiotic associations changed at the same time that these clades became relatively more abundant. Loss or reduction in $\delta^{13}C$ enrichment across the PETM is more likely driven by changes in the nature of photosymbiotic associations (i.e., changes in photosymbiont load, activity, effect, location or type) than modern-type bleaching, given the long timescales involved (spanning many generations of populations), spatial heterogeneity in signal before the event, and heterogeneity in response to the event. Such flexibility in photosymbiont associations may contribute to the relative success of photosymbiont-bearing taxa during the PETM and provide a note of hope for our current biodiversity crisis in attesting the resilience of some photosymbiont-bearing species.

Acknowledgments

We thank B. Erkkila and M. Wint of the Yale Analytical and Stable Isotope Center, C. Charles at the UCSD Stable Isotope Laboratory, and D. Andreasen at the UCSC Stable Isotope Laboratory for help with isotopic analyses; G. Dickens and four anonymous reviewers for insightful comments which improved our article; and the International Ocean Discovery Program for samples from Sites ODP 1209, ODP 690, and DSDP 401. E.T. recognizes funding by National Science Foundation (NSF) OCE 1536611. P.M.H., S.D., and J.O.S recognize funding by NSF OCE 1536604 and a Sloan Research Fellowship. Work on isotopic records at DSDP 401 and ODP 690 was part of J.A.L.'s M.S. thesis under R.D.N. The authors declare no competing interests.

Data Availability Statement

Supplementary materials, isotopic data, and assemblage data available at https://doi.pangaea.de/10.1594/PANGAEA.918702.

Literature Cited

Aze, T., P. N. Pearson, A. J. Dickson, M. P. S. Badger, P. R. Bown, R. D. Pancost, S. J. Gibbs, B. T. Huber, M. J. Leng, A. L. Coe, A. S. Cohen, and G. L. Foster. 2014. Extreme warming of tropical waters during the Paleocene–Eocene thermal maximum. Geology 42:739–742.

Bains, S., R. M. Corfield, and R. D. Norris. 1999. Mechanisms of climate warming at the end of the Paleocene. Science 285:724–727.

Bard, E. 2001. Paleoceanographic implications of the difference in deepsea sediment mixing between large and fine particles. Paleoceanography 16:235–239.

Birch, H., H. K. Coxall, P. N. Pearson, D. Kroon, and M. O'Regan. 2013. Planktonic foraminifera stable isotopes and water column structure: disentangling ecological signals. Marine Micropaleontology 101:127–145.

Bird, C., K. F. Darling, A. D. Russell, C. V. Davis, J. Fehrenbacher, A. Free, M. Wyman, and B. T. Ngwenya. 2017. Cyanobacterial endobionts within a major marine planktonic calcifier (*Globigerina bulloides*, Foraminifera) revealed by 16S rRNA metabarcoding. Biogeosciences 14:901–920.

Bornemann, A., R. D. Norris, J. A. Lyman, S. D'haenens, J. Groeneveld, U. Röhl, K. A. Farley, and R. P. Speijer. 2014. Persistent environmental change after the Paleocene–Eocene Thermal Maximum in the eastern North Atlantic. Earth and Planetary Science Letters 394:70–81.

Bornemann, A., S. D'haenens, R. D. Norris, and R. P. Speijer. 2016. The demise of the early Eocene greenhouse—decoupled deep and surface water cooling in the eastern North Atlantic. Global and Planetary Change 145:130–140.

Bralower, T. J. 2002. Evidence of surface water oligotrophy during the Paleocene–Eocene thermal maximum: nannofossil assemblage data from Ocean Drilling Program Site 690, Maud Rise, Weddell Sea. Paleoceanography 17:13-1–13-12.

Cramer, B. S., J. D. Wright, D. V. Kent, and M. P. Aubry. 2003. Orbital climate forcing of δ13C excursions in the late Paleocene–early Eocene (chrons C24n-C25n). Paleoceanography 18.

D'Haenens, S., A. Bornemann, K. Roose, P. Claeys, and R. P. Speijer. 2012. Stable isotope paleoecology (δ13C and δ18O) of early Eocene *Zeauvigerina aegyptiaca* from the north Atlantic (DSDP site 401). Austrian Journal of Earth Sciences 105:179–188.

D'Hondt, S., J. C. Zachos, G. Schultz, and N. Summer. 1994. Stable isotopic signals and photosymbiosis in late Paleocene planktic foraminifera. 20:391–406.

Donner, S. D., W. J. Skirving, C. M. Little, M. Oppenheimer, and O. Hoegh-Gulberg. 2005. Global assessment of coral bleaching and required rates of adaptation under climate change. Global Change Biology 11:2251–2265.

Dunkley Jones, T., D. J. Lunt, D. N. Schmidt, A. Ridgwell, A. Sluijs, P. J. Valdes, and M. Maslin. 2013. Climate model and proxy data constraints on ocean warming across the Paleocene–Eocene Thermal Maximum. Earth-Science Reviews 125:123–145.

Dutton, A., K. C. Lohmann, and R. M. Leckie. 2005. Insights from the Paleogene tropical Pacific: foraminiferal stable isotope and elemental results from Site 1209, Shatsky Rise. Paleoceanography 20:1–16.

Edgar, K. M., S. M. Bohaty, S. J. Gibbs, P. F. Sexton, R. D. Norris, and P. A. Wilson. 2013. Symbiont "bleaching" in planktic foraminifera during the Middle Eocene Climatic Optimum. Geology 41:15–18.

Edgar, K. M., P. M. Hull, and T. H. G. Ezard. 2017. Evolutionary history biases inferences of ecology and environment from $\delta^{13}C$ but not $\delta^{18}O$ values. Nature Communications 8:1–9.

Ezard, T. H. G., K. M. Edgar, and P. M. Hull. 2015. Environmental and biological controls on size-specific $\delta^{13}C$ and $\delta^{18}O$ in recent planktonic foraminifera. Paleoceanography 30:151–173.

Frieling, J., G.-J. Reichart, J. J. Middelburg, U. Röhl, T. Westerhold, S. M. Bohaty, and A. Sluijs. 2017. Tropical Atlantic climate and ecosystem regime shifts during the Paleocene–Eocene Thermal Maximum. Climate of the Past 14:39–55.

Gaskell, D. E., and P. M. Hull. 2019. Symbiont arrangement and metabolism can explain high δ13C in eocene planktonic foraminifera. Geology 47:1156–1160.

Gibbs, S. J., P. R. Bown, B. H. Murphy, A. Sluijs, K. M. Edgar, H. Pälike, C. T. Bolton, and J. C. Zachos. 2012. Scaled biotic disruption during early Eocene global warming events. Biogeosciences 9:4679–4688.

Gutjahr, M., A. Ridgwell, P. F. Sexton, E. Anagnostou, P. N. Pearson, H. Pälike, R. D. Norris, E. Thomas, and G. L. Foster. 2017. Very large release of mostly volcanic carbon during the Palaeocene–Eocene Thermal Maximum. Nature 548:573–577.

Hallock, P., D. E. Williams, E. M. Fisher, and S. K. Toler. 2006. Bleaching in foraminifera with algal symbionts: implications for reef monitoring and risk assessment. Anuario do Instituto de Geociencias 29:108–128.

Hay, W. W., R. M. DeConto, C. N. Wold, K. M. Wilson, S. Voigt, M. Schulz, A. R. Wold, W.-C. Dullo, A. B. Ronov, A. N. Balukhovsky, and E. Söding. 1999. Alternative global Cretaceous paleogeography. *In* E. Barrera and C. C. Johnson, eds. Evolution of the Cretaceous ocean-climate system. Geological Society of America Special Paper 332: 1–47.

Henehan, M. J., G. L. Foster, H. C. Bostock, R. Greenop, B. J. Marshall, and P. A. Wilson. 2016. A new boron isotope-pH calibration for *Orbulina universa*, with implications for understanding and accounting for "vital effects." Earth and Planetary Science Letters 454:282–292.

Henehan, M. J., K. M. Edgar, G. L. Foster, D. E. Penman, P. M. Hull, R. Greenop, E. Anagnostou, and P. N. Pearson. 2020. Revisiting the Middle Eocene Climatic Optimum "carbon cycle conundrum" with new estimates of atmospheric pCO_2 from boron isotopes. Paleoceanography and Paleoclimatology 35:e2019PA003713.

Hughes, T. P., J. T. Kerry, A. H. Baird, S. R. Connolly, A. Dietzel, C. M. Eakin, S. F. Heron, A. S. Hoey, M. O. Hoogenboom, G. Liu, M. J. McWilliam, R. J. Pears, M. S. Pratchett, W. J. Skirving, J. S. Stella, and G. Torda. 2018. Global warming transforms coral reef assemblages. Nature 556:492–496.

Hull, P. M., P. J. S. Franks, and R. D. Norris. 2011. Mechanisms and models of iridium anomaly shape across the Cretaceous–Paleogene boundary. Earth and Planetary Science Letters 301:98–106.

Hupp, B. N., and D. C. Kelly. 2020. Delays, discrepancies, and distortions: Size-dependent sediment mixing and the deep-sea record of the Paleocene–Eocene Thermal Maximum from ODP Site 690 (Weddell Sea). Paleoceanography and Paleoclimatology 35:e2020PA004018.

Hupp, B. N., D. C. Kelly, J. C. Zachos, and T. J. Bralower. 2019. Effects of size-dependent sediment mixing on deep-sea records of the Paleocene–Eocene Thermal Maximum. Geology 47:749–752.

Katz, M. E., D. R. Katz, J. D. Wright, K. G. Miller, D. K. Pak, N. J. Shackleton, and E. Thomas. 2003. Early Cenozoic benthic foraminiferal isotopes: species reliability and interspecies correction factors. Paleoceanography 18. doi: 10.1029/2002PA000798

Kelly, D. C. 2002. Response of Antarctic (ODP Site 690) planktonic foraminifera to the Paleocene–Eocene thermal maximum: faunal evidence for ocean/climate change. Paleoceanography 17:23-1–23-13.

Kelly, D. C., T. J. Bralower, J. C. Zachos, I. P. Silva, and E. Thomas. 1996. Rapid diversification of planktonic foraminifera in the tropical Pacific (ODP Site 865) during the late Paleocene thermal maximum. Geology 24:423–426.

Kelly, D. C., J. C. Zachos, T. J. Bralower, and S. A. Schellenberg. 2005. Enhanced terrestrial weathering/runoff and surface ocean carbonate production during the recovery stages of the Paleocene–Eocene thermal maximum. Paleoceanography 20. doi: 10.1029/2005PA001163.

Kelly, D. C., T. M. J. Nielsen, and S. A. Schellenberg. 2012. Carbonate saturation dynamics during the Paleocene–Eocene thermal maximum: bathyal constraints from ODP sites 689 and 690 in the Weddell Sea (South Atlantic). Marine Geology 303:75–86.

Kennett, J. P., and L. D. Stott. 1991. Abrupt deep-sea warming, palaeoceanographic changes and benthic extinctions at the end of the Palaeocene. Nature 353:225–229.

Kirtland Turner, S. 2018. Constraints on the onset duration of the Paleocene–Eocene Thermal Maximum. Philosophical Transactions of the Royal Society of London A 376:20170082.

Kirtland Turner, S., P. M. Hull, L. R. Kump, and A. Ridgwell. 2017. A probabilistic assessment of the rapidity of PETM onset. Nature Communications 8:1–10.

Kopp, R. E., D. Schumann, T. D. Raub, D. S. Powars, L. V. Godfrey, N. L. Swanson-Hysell, A. C. Maloof, and H. Vali. 2009. An Appalachian Amazon? Magnetofossil evidence for the development of a tropical river-like system in the mid-Atlantic United States during the Paleocene–Eocene thermal maximum. Paleoceanography 24. doi: 10.1029/2009PA001783.

Lombard, F., R. E. da Rocha, J. Bijma, and J. P. Gattuso. 2009. Effect of carbonate ion concentration and irradiance on calcification in foraminifera. Biogeosciences Discussions 6:8589–8608.

Luciani, V., R. D'Onofrio, G. R. Dickens, and B. S. Wade. 2017. Did photosymbiont bleaching lead to the demise of planktic foraminifer *Morozovella* at the Early Eocene Climatic Optimum? Paleoceanography 32:1115–1136.

Norris, R. D. 1998. Recognition and macroevolutionary significance of photosymbiosis in molluscs, corals, and foraminifera. Paleontological Society Papers 4:68–100.

Nunes, F., and R. D. Norris. 2006. Abrupt reversal in ocean overturning during the Palaeocene/Eocene warm period. Nature 439:60–63.

Pandolfi, J. M., and W. Kiessling. 2014. Gaining insights from past reefs to inform understanding of coral reef response to global climate change. Current Opinion in Environmental Sustainability 7:52–58.

Pardo, A., G. Keller, E. Molina, and J. I. Canudo. 1997. Planktic foraminiferal turnover across the Paleocene–Eocene transition at DSDP Site 401, Bay of Biscay, North Atlantic. Marine Micropaleontology 29:129–158.

Pearson, P. N., P. W. Ditchfield, J. Singano, K. G. Harcourt-Brown, C. J. Nicholas, R. K. Olsson, N. J. Shackleton, and M. A. Hall. 2001. Warm tropical sea surface temperatures in the Late Cretaceous and Eocene epochs. Nature 413:481–487.

Pearson, P. N., R. K. Olsson, B. T. Huber, C. Hemleben, and W. A. Berggren. 2006. Atlas of Eocene planktonic foraminifera. Cushman Foundation for Foraminiferal Research Special Publication 41:513.

Penman, D. E., B. Hönisch, R. E. Zeebe, E. Thomas, and J. C. Zachos. 2014. Rapid and sustained surface ocean acidification during the Paleocene–Eocene Thermal Maximum. Paleoceanography 29:357–369.

Petrizzo, M. R. 2007. The onset of the Paleocene–Eocene Thermal Maximum (PETM) at Sites 1209 and 1210 (Shatsky Rise, Pacific Ocean) as recorded by planktonic foraminifera. Marine Micropaleontology 63:187–200.

Plaziat, J. C., and C. Perrin. 1992. Multikilometer-sized reefs built by foraminifera (*Solenomeris*) from the early Eocene of the Pyrenean domain (S. France, N. Spain): palaeoecologic relations with coral

reefs. Palaeogeography, Palaeoclimatology, Palaeoecology 96:195–231.
Prazeres, M. 2018. Bleaching-associated changes in the microbiome of large benthic foraminifera of the Great Barrier Reef, Australia. Frontiers in Microbiology 9:2404.
Rowan, R. 2004. Coral bleaching: thermal adaptation in reef coral symbionts. Nature 430:742–742.
Santavy, D. L., J. K. Summers, V. D. Engle, and L. C. Harwell. 2005. The condition of coral reefs in South Florida (2000) using coral disease and bleaching as indicators. Environmental Monitoring and Assessment 100:129–152.
Scheibner, C., and R. P. Speijer. 2008. Late Paleocene–early Eocene Tethyan carbonate platform evolution—a response to long-and short-term paleoclimatic change. Earth-Science Reviews 90:71–102.
Schiebel, R. 2002. Planktic foraminiferal sedimentation and the marine calcite budget. Global Biogeochemical Cycles 16:1–21.
Schiebel, R., and C. Hemleben. 2017. Planktic foraminifers in the modern ocean. Springer, Berlin.
Schmidt, C., D. Titelboim, J. Brandt, B. Herut, S. Abramovich, A. Almogi-Labin, and M. Kucera. 2016. Extremely heat tolerant photo-symbiosis in a shallow marine benthic foraminifera. Scientific Reports 6:30930.
Schmidt, C., R. Morard, O. Romero, and M. Kucera. 2018. Diverse internal symbiont community in the endosymbiotic foraminifera *Pararotalia calcariformata*: implications for symbiont shuffling under thermal stress. Frontiers in Microbiology 9. doi: 10.3389/fmicb.2018.02018.
Si, W., and M. P. Aubry. 2018. Vital effects and ecologic adaptation of photosymbiont-bearing planktonic foraminifera during the Paleocene–Eocene thermal maximum, implications for paleoclimate. Paleoceanography and Paleoclimatology 33:112–125.
Simpson, C., W. Kiessling, H. Mewis, R. C. Baron-Szabo, and J. Müller. 2011. Evolutionary diversification of reef corals: a comparison of the molecular and fossil records. Evolution 65:3274–3284.
Sluijs, A., and G. R. Dickens. 2012. Assessing offsets between the $\delta^{13}C$ of sedimentary components and the global exogenic carbon pool across early Paleogene carbon cycle perturbations. Global Biogeochemical Cycles 26. doi: 10.1029/2011GB004224.
Speijer, R. P., C. Scheibner, P. Stassen, and A. M. M. Morsi. 2012. Response of marine ecosystems to deep-time global warming: a synthesis of biotic patterns across the Paleocene–Eocene thermal maximum (PETM). Austrian Journal of Earth Sciences 105:6–16.
Spero, H. J. 1998. Life history and stable isotope geochemistry of planktonic foraminifera. Paleontological Society Papers 4:7–36.
Spero, H. J., and M. DeNiro. 1987. The influence of symbiont photosynthesis on the $\delta^{18}O$ and $\delta^{13}C$ values of planktonic foraminiferal shell calcite. Symbiosis 4:213–228.
Spero, H. J., I. Lerche, and D. F. Williams. 1991. Opening the carbon isotope "vital effect" black box, 2, quantitative model for interpreting foraminiferal carbon isotope data. Paleoceanography 6:639–655.
Spero, H. J., J. Bijma, D. W. Lea, and B. E. Bemis. 1997. Effect of seawater carbonate concentration on foraminiferal carbon and oxygen isotopes. Nature 390:497–500.
Spezzaferri, S., A. El Kateb, C. Pisapia, and P. Hallock. 2018. In situ observations of foraminiferal bleaching in the Maldives, Indian Ocean. Journal of Foraminiferal Research 48:75–84.
Stanley, G., and B. van de Schootbrugge. 2018. The evolution of the coral–algal symbiosis and coral bleaching in the geologic past. Pp. 9–26 *in* M. J. H. van Oppen, Madeleine and J. Lough, eds. Coral bleaching: patterns, processes, causes and consequences. Springer International, Cham, Switzerland.
Stap, L., L. Lourens, A. Van Dijk, S. Schouten, and E. Thomas. 2010. Coherent pattern and timing of the carbon isotope excursion and warming during Eocene Thermal Maximum 2 as recorded in planktic and benthic foraminifera. Geochemistry, Geophysics, Geosystems 11. doi: 10.1029/2010GC003097.
Stassen, P., R. P. Speijer, and E. Thomas. 2014. Unsettled puzzle of the Marlboro clays. Proceedings of the National Academy of Sciences USA 111:e1066–e1067.
Sugarman, P. J., K. G. Miller, J. V. Browning, P. P. McLaughlin, G. J. Brenner, B. Buttari, B. S. Cramer, A. Harris, J. Hernandez, M. E. Katz, B. Lettini, S. Misintseva, D. H. Monteverde, R. K. Olsson, L. Patrick, E. Roman, M. J. Wojtko, M. Aubry, M. D. Feigenson, J. A. Barron, S. Curtin, G. Cobbs, G. Cobbs III, D. Bukry, and B. A. Huffman. 2005. Millville Site. Proceedings of the Ocean Drilling Program, Initial Reports 174AX (Suppl):1–94. College Station, Tex.
Takagi, H., K. Kimoto, T. Fujiki, and K. Moriya. 2018. Effect of nutritional condition on photosymbiotic consortium of cultured *Globigerinoides sacculifer* (Rhizaria, Foraminifera). Symbiosis 76:25–39.
Takagi, H., K. Kimoto, T. Fujiki, H. Saito, C. Schmidt, M. Kucera, and K. Moriya. 2019. Characterizing photosymbiosis in modern planktonic foraminifera. Biogeosciences 16:3377–3396.
Takeda, K., and K. Kaiho. 2007. Faunal turnovers in central Pacific benthic foraminifera during the Paleocene–Eocene thermal maximum. Palaeogeography, Palaeoclimatology, Palaeoecology 251:175–197.
Thomas, D. J., J. C. Zachos, T. J. Bralower, E. Thomas, and S. Bohaty. 2002. Warming the fuel for the fire: evidence for the thermal dissociation of methane hydrate during the Paleocene–Eocene thermal maximum. Geology 30:1067.
Thomas, E., 2003. Extinction and food at the sea floor: a high-resolution benthic foraminiferal record across the initial Eocene Thermal Maximum, Southern Ocean Site 690. *In* S. Wing, P. Gingerich, B. Schmitz, and E. Thomas, eds. Causes and consequences of globally warm climates of the Paleogene. Geological Society of America Special Paper 369:319–332.
Thomas, E., and N. J. Shackleton. 1996. The Paleocene–Eocene benthic foraminiferal extinction and stable isotope anomalies. Geological Society of London Special Publication 101:401–441.
Thomas, E., J. Zachos, and T. Bralower. 2000. Deep-sea environments on a warm earth: latest Paleocene–early Eocene. Pp. 132–160 *in* B. Huber, K. MacLeod, and S. Wing, eds. Warm climates in earth history. Cambridge University Press, Cambridge.
Tripati, A., and H. Elderfield. 2005. Deep-sea temperature and circulation changes at the Paleocene–Eocene Thermal Maximum. Science 308:1894–1898.
Wade, B. S., N. Al-Sabouni, C. Hemleben, and D. Kroon. 2008. Symbiont bleaching in fossil planktonic foraminifera. Evolutionary Ecology 22:253–265.
Weiss, A. M., and R. C. Martindale. 2019. Paleobiological traits that determined scleractinian coral survival and proliferation during the late Paleocene and early Eocene hyperthermals. Paleoceanography and Paleoclimatology 34:252–274.
Westerhold, T., U. Röhl, B. Donner, H. K. Mccarren, and J. C. Zachos. 2011. A complete high-resolution Paleocene benthic stable isotope record for the central Pacific (ODP Site 1209). Paleoceanography 26:1–13.
Winguth, A. M. E., E. Thomas, and C. Winguth. 2012. Global decline in ocean ventilation, oxygenation, and productivity during the Paleocene–Eocene Thermal Maximum: implications for the benthic extinction. Geology 40:263–266.
Zachos, J. C., M. W. Wara, S. Bohaty, M. L. Delaney, M. R. Petrizzo, A. Brill, T. J. Bralower, and I. Premoli-Silva. 2003. A transient rise in tropical sea surface temperature during the Paleocene–Eocene thermal maximum. Science 302:1551–1554.
Zeebe, R. E., J. Bijma, and D. a Wolf-Gladrow. 1999. A diffusion-reaction model of carbon isotope fractionation in foraminifera. Marine Chemistry 64:199–227.